Impacts of Soil Properties on Bluff Recession under Combined Waves and Surge Actions: An Experimental Study with Uncertainty Quantification

Ali Farhadzadeh*, Mahsa Ghazian Arabi, Tao Xiang

Department of Civil Engineering, College of Engineering and Applied Sciences, Stony Brook University, Stony Brook, 11794, New York, USA.

ABSTRACT

Soil mixtures with five fines contents, two water contents, and two relative densities underwent soil mechanics tests to quantify their strength indices. The soil was then molded to create small-scale steep beaches and bluff models subjected to varying water levels and waves in a wave flume. The equilibrium beach profile of the model containing a higher fines content, higher relative density, and the optimum water content, followed a concave down profile, while that of the models with the lower density and/or lower fines content, was concave up. The bluffs composed of the materials with the optimum water content exhibited a reduced crest recession compared to those with the constituent materials dry of optimum. The recession rate of the bluff crest decreased with the increase of the effective cohesion. For a given effective cohesion, the recession rate was significantly influenced by the relative density. The impact of the effective cohesion on the recession rate for the bluff composed of the looser soil was significantly greater than that of the bluffs with the denser constituent material. Furthermore, the uncertainty associated with the effects of the variations in the fines content, relative density, and water content on the recession rate was quantified.

*Corresponding author
Email address: ali.farhadzadeh@stonybrook.edu (Ali Farhadzadeh)

1. INTRODUCTION

Erosion of steep shores and failure and recession of coastal bluffs can pose major hazards to coastal communities and entail economic, environmental and societal consequences. A host of factors contribute to the complexity in predicting the response of such land features to the environmental forcing, concerning interactions among land- and sea-based agents (Buckler & Winters, 1983; Carter et al., 1987; Vallejo & Degroot, 1988; Swenson et al., 2006; Castedo et al., 2013). The mechanical strength of the beach-bluff system's constituent materials in connection with the slope stability of steep shores and bluff can significantly influence their behavior under hydrodynamic forcing by waves and surges (Collins & Sitar, 2008, 2009; Trenhaile, 2009; Ghazian Arabi et al., 2020a, 2020b). The erosion of cohesive materials has been studied by many researchers (e.g., Kamphuis, 1990; Rohan et al., 1980; Skafel & Bishop, 1994; Sunamura, 1976, Damgaard & Dong, 2004; Newson et al., 2006). However, detailed studies focusing on the impacts of the constituent material properties, such as composition, relative density, water content—tied to the soil strength—on the erosion responses of sloping shores are still lacking.

Water content, for example, influences the electrochemical forces among fine-grained particles and the frictional and interlocking forces among coarse-grained aggregates, all of which can alter the material's strength (Holtz et al., 2003). Bonds of various strengths forming among the particles of soils, compacted at different moisture ratios can influence the soil erodibility (Wan & Fell, 2004). Mitchener & Torfs (1996) stated that the erosion resistance of sand-mud mixtures is greater than that of each sand or mud, separately; and that a soil mixture with a mud content between 3% to 15% changes behaves like a cohesive sediment. van Ledden et al. (2004) introduced the concept of critical mud content based on which the soil behavior can be classified into cohesive and cohesionless. They authors concluded that a soil with mud fraction larger than the critical mud content exhibits behaviors analogous to cohesive soils. Farhadzadeh & Ghazian Arabi (2020) established a linkage between the water content and stiffness of the low-fines content soils and their initiation of erosion. Ghazian Arabi & Farhadzadeh (2022) showed that

the increase of the fines content in the soil results in an increase of the effective cohesion and decrease of the effective angle of internal friction. The increase of the effective cohesion was more significant for soils with a higher density/packing, particularly those prepared at the optimum water content. Their results showed a meaningful increase of the soil erosion resistance with the increase of fines content and relative density. Ghazian Arabi et al. (2020a, 2020b) who performed a thorough review of the literature on bluff erosion, presented an analysis of their laboratory work outlying the recession mechanisms for predominantly sandy bluffs. The present work discusses the most recent progresses the authors have made in understanding and quantifying the erosion of steep beaches and recession bluffs of low fines content, subjected to breaking wave and rising surge actions in relation to the constituent material properties.. To that end, laboratory experiments, including the soil mechanics and wave flume tests, were carried out on a broader range of variables that influence the mechanical properties of bluff forming materials. The materials included low fines content soils of various compositions, initial water contents and relative densities. The flume experiments led to the development of empirical relationship for the recession rate of the bluff as a function of the soil properties. An uncertainty analysis was carried to unravel the impacts of variations in the material properties on the recession rate.

This study aims to develop a better understanding of how heterogeneity in the bluff forming material can influence its erosion and recession processes under wave and surge forcing—which is currently lacking in the literature. Such information can lead to science-based coastal zone management and disaster mitigation in bluff-dominated coasts.

2. MATERIAL AND METHOD

A series of tests were carried out in the soil mechanics laboratory to quantify the compositions and strength indices of the bluff forming materials collected from Montauk on Long Island, New York. The soil from the study area is predominantly sandy with small fraction (~20%) fine-grained material (Ghazian Arabi et al., 2018). The fine material is composed of more than 40% Illite and less than 25%

Chlorite and Kaolinite, each (Lonnie, 1977). Specimens of different strengths were reconstituted for the flume experiments. The constituent material properties of the specimens reflected the range of variations of the soil in the field. These soil mixtures were then used to construct beach and bluff profiles in a small wave flume. The flume tests, at a scale of approximately 1:100, included 20 beach-bluff profiles composed of various fines contents, relative densities, and water contents exposed to regular incident waves and a rising surge.

2.1. Material characteristics

Ghazian Arabi et al. (2020b) analyzed the experimental test results for eight soil mixtures which included four different fines contents, ξ_f= 0, 5, 10, and 15%—equivalent to four coarse content ξ_{sa}=100, 95, 90, and 85%, respectively— prepared with two relative densities, D_r = 39% and 68%, referred to herein as the looser (L) and denser (D), respectively. All the eight soil mixtures had a constant water content (ω=7%)—dry of optimum. The present work extends and generalize the authors' previous study through a more comprehensive experimental campaign. Twelve new beach-bluff models, consisted of two having ξ_f= 20%, D_r= 39, 68%, and ω = 7% (i.e., Cases: C20L, C20D) and ten beach-bluffs with the same fines to sand ratios as those of the dry samples (i.e., ξ_f= 0 to 20%, at a 5% increment), but with a moisture ratio according to the optimum water content ($\omega = \omega_{opt}$) of each soil mixture (indicated using the letter W at the beginning of their names), to two relative densities, D_r= 39, 68% (i.e., Cases: WC0L, WC5L, WC10L, WC15L, WC20L, WC0D, WC5D, WC10D, WC15D, and WC20D). Tables 1 and 2 list the important characteristics of the soil mixtures including their classifications according to the Unified Soil Classification System (USCS) based on which the soil mixtures with $\xi_f < 5\%$ are classified as poorly graded sand (SP) and those with $\xi_f > 12\%$ are clayey sand (SC). The soil mixtures with $5\% < \xi_f < 12\%$ are categorized as poorly graded sand with clay (SP-SC).

The Standard Proctor Compaction test (ASTM D698-12e2, 2012) was carried out to determine the optimum water content and corresponding dry unit weight (γ_d) of each soil. As summarized in Tables

1 and 2, the optimum water content ranges between $\omega_{opt} = 9.5\%$, for the soil mixtures with the soil mixture with the lowest ($\xi_f = 0$), and $\omega_{opt} = 13.2\%$, for that of highest fines content ($\xi_f = 20\%$). The results indicate that ω_{opt} and γ_d increase with ξ_f. Tables 2 summarizes the optimum water contents.

Table 1. Specifications of soil mixtures prepared at water content dry of optimum

No.	Name	ξ_f (%)	ξ_{sa} (%)	ω (%)	D_r (%)	ρ_b (kg/m^3)	C' (kPa)	ϕ' (°)	C (kPa)	ϕ (°)	USCS
1	C0L	0	100	7	39	1776	0.00	33.0	0.00	32.5	SP
2	C5L	5	95	7	39	1776	1.01	31.2	1.75	28.5	SP-SC
3	C10L	10	90	7	39	1776	2.17	26.5	2.81	25.7	SP-SC
4	C15L	15	85	7	39	1776	3.20	26.4	3.35	25.3	SC
5	C20L	20	80	7	39	1776	5.12	22.1	4.55	20.1	SC
6	C0D	0	100	7	68	1927	0.00	34.3	0.00	33.9	SP
7	C5D	5	95	7	68	1927	1.95	32.1	2.13	31.9	SP-SC
8	C10D	10	90	7	68	1927	3.47	31.3	3.62	30.4	SP-SC
9	C15D	15	85	7	68	1927	4.23	29.7	4.53	28.9	SC
10	C20D	20	80	7	68	1927	4.93	27.2	5.27	25.2	SC

Table 2. Specification of soil mixtures prepared at optimum water contents

No.	Name	ξ_f (%)	ξ_{sa} (%)	$\omega = \omega_{opt}$ (%)	D_r (%)	ρ_b (kg/m^3)	C' (kPa)	ϕ' (°)	C (kPa)	ϕ (°)	USCS
11	WC0L	0	100	9.5	39	1817	0.00	33.3	0.00	32.8	SP
12	WC5L	5	95	10.2	39	1829	1.26	32.8	2.19	29.4	SP-SC
13	WC10L	10	90	11.0	39	1842	3.25	27.2	4.22	26.9	SP-SC
14	WC15L	15	85	12.8	39	1872	4.12	26.7	4.32	25.6	SC
15	WC20L	20	80	13.2	39	1879	5.17	22.4	5.69	21.2	SC
16	WC0D	0	100	9.5	68	1972	0.00	34.6	0.00	34.2	SP
17	WC5D	5	95	10.2	68	1985	2.24	32.4	2.56	32.7	SP-SC
18	WC10D	10	90	11.0	68	1999	4.16	32.3	4.71	31.6	SP-SC
19	WC15D	15	85	12.8	68	2031	5.20	30.1	5.89	29.2	SC
20	WC20D	20	80	13.2	68	2039	5.96	27.6	6.53	26.1	SC

The mechanical strength of the soil mixtures were determined using the Consolidated Undrained (CU) triaxial testing (ASTM D4767-11, 2011) and by developing the Mohr-Coulomb failure criterion for each soil mixture. A total of 60 triaxial, three tests for each soil mixture, were carried out. The Mohr-

Coulomb failure criterion provides both the total and effective cohesions (C and C', respectively) and total and effective angles of internal friction (ϕ and ϕ' and, respectively) which, in combination, describe the mechanical strength of the soil. Tables 1 and 2 list the summary of the Mohr-Coulomb failure criteria for all soil mixtures. The effective cohesion increases with the fines content and that increase is more pronounced for the denser soil compacted at the optimum water content.

2.2. Flume experiment setup and procedure

The bluff model was constructed in a flume that was 3.6 m long, 11 cm wide and 30 cm deep, and equipped with a flap-type paddle that generated monochromatic waves (Figure 1). The wave flume experiments involved exposing the model steep beach and a vertical-front bluff system to varying sinusoidal waves and a staged rising surge, for a total duration of 36 hours. The beach in front of the bluff of 9 cm high had a steep slope of $tan(\theta) = 1/4.2$ ($i.e., \theta \sim 13^{\circ}$) extending 55 cm in the offshore direction, from the bluff toe. The model beach-bluff was constructed layer by layer under a carefully controlled condition. Initially, soil compaction calibration procedure for staged construction (Ladd, 1978) was carried out to ensure the density uniformity of the beach and bluff model. Subsequently, the material was prepared at the target composition and moisture ratio and placed in the mold in a layer of a few centimeters in an in-situ mold and compacted to the target density (considering the mass of the soil and volume of the mold). This procedure was continued until the entire model was constructed. After removing the mold, the flume was gradually filled with water until the still water level reached 1.5 cm below the bluff toe (η = -1.5 cm) which corresponds to Phase 1. The steep beach and bluff were subjected, for a duration of for t_d =12 hours, to the monochromatic waves with a height and period of H = 4.5 cm and T = 0.51 s, respectively. For Phase 2, the water level was risen 1 cm (i.e., η = -0.5 cm). The wave height was increased by ~30% to H = 5.8 cm and lasted for another 12 hours. Subsequently, in Phase 3, the surge level was risen to η = 0.5 cm and the wave heigh was increased nearly 16% to H = 6.7 cm attacking the beach and bluff for an additional 12 hours. The wave period during the three phases

remained constant (T = 0.51 s) and the breaker type was categorized as plunging (Battjes, 1974). The wave and surge characteristics as well as the breaker type for the three phases of the test are listed in Table 3. The wave was measured offshore of the steep slope, using a high-resolution resistive wave gauge sampling the water surface fluctuations at a rate of 128 Hz.

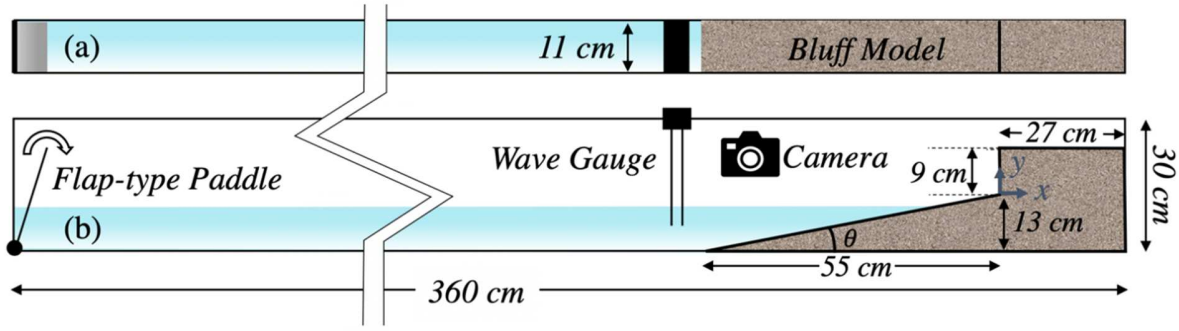

Figure 1. Schematic of experimental setup for wave flume tests

Table 3. Specifications of wave and surge during each phase

Phase	Surge	Wave			Duration	Breaking type
	η (cm)	H (cm)	T (s)	L (cm)	t_d (hour)	
1	-1.5	4.5	0.51	38.7	12	Plunging
2	-0.5	5.8	0.51	39.1	12	
3	0.5	6.7	0.51	39.5	12	

2.3. Beach and bluff profile measurements using image processing

A GoPro Hero5 Black camera captured the image of the surface profile of the beach and bluff model, through the flume's transparent sidewall. The images were digitized using various MATLAB R2017a image processing toolboxes and the bottom profile of the beach and the face of the bluff were extracted. Before beginning to capture the pictures, the camera was calibrated using the Camera Calibrator toolbox with the aid of gridded sheets of a known grid size. The camera recorded the images at a frequency of 0.1 Hz. The images were projected into the X-Y coordinates (Figure 2) and processed in

three steps to detect the profiles (Figure 3). The profiles were first detected using the Color Thresholder toolbox (Figure 3-Figure A). Subsequently, the Image Region Analyzer toolbox was employed to delete and eliminate the noise. The noise could be dirty spots on the side wall and muddy water (Figure 3-B). Finally, the Image Segmentation toolbox was utilized to eliminate the unnecessary information, such as the background color and the bluff's rear edge (Figure 3-C). These data provided information regarding how the beach and bluff evolve in response to the varying wave and surge actions, during the 36-hour duration of each test.

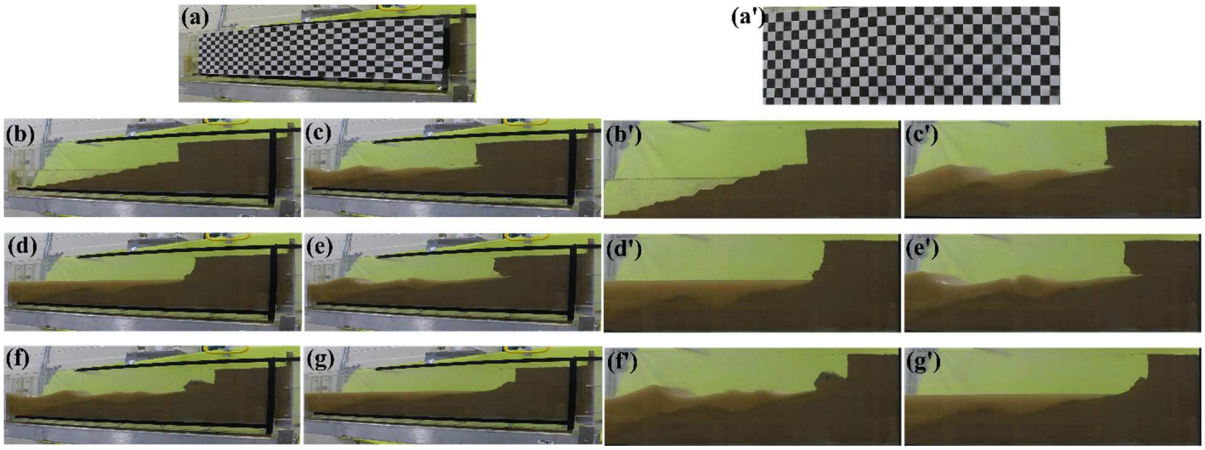

Figure 2. Example of projection of images to X-Y coordinates, (a)-(g) original images, and (a')-(g') projected images.

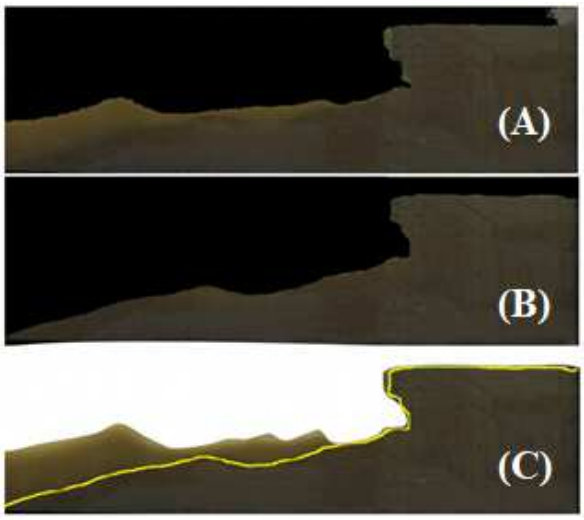

Figure 3. Different steps of image processing: (A) color threshold technique, (B) region analyzing and image segmentation, and (C) overlay of detected edge on original image.

3. RESULTS AND DISCUSSIONS

The processes controlling the recession rate of the bluffs by the breaking waves and rising surge are discussed. The processes include the foreshore erosion, offshore transport and deposition of the material from the beach and failed bluff deposits. The analyses include both spatial and temporal changes of the profile data extracted from the images using the non-intrusive image processing technique described above. In addition, an uncertainty analysis has been carried out to further assess the impacts of variations in the constituent material on the recession rate is performed.

3.1. *General process of beach erosion and bluff recession*

The flume tests consisted of the initial planar beach adjustments by incident waves to an equilibrium state for the set surge level (Ghazian Arabi et al. 2020b). In Phase 1, the surge level was the lowest and the steep planar beach subjected to the wave actions for 12 hours. This resulted in a semi-equilibrium beach profile. During Phases 2 and 3 the beach material eroded by the breaking wave and resulting swash flow actions was transported offshore by the undertow current. Consequently, the wave runup was able to reach further landward and remove the sediment from the bluff face and form a notch at its toe. The

development and progression of the notch on some occasions, especially when the material had a lower mechanical strength, resulted in the slope instability and failure, and bluff crest recession. Following the failure, the sediment deposit on the beach was transported and deposited offshore by the combined swash and undertow flow. These processes eventually led to an equilibrium beach profile in each Phase, before the surge level was increased at the beginning of the subsequent phase. The time required for the equilibrium state varied in each Phase and for each soil.

3.2. *Analyses of beach and bluff profiles*

Figure 4 illustrates the profile evolutions for all the bluff models with the constituent materials listed in Tables 1 and 2. The foreshore erosion, bluff failure, sediment deposit at the bluff toe, transport of the deposit offshore, and formation of sandbar are trackable using the color scale. The sharp, stepwise color change from a darker to a lighter color near the toe ($X = 0\ cm$) marks the occurrence of episodic bluff failure and recession. In general, the bluff failure occurs short after the rise of the water level (i.e., ~ $t =$ 12 and 24 h, in Phases 2 and 3, respectively), except for the bluff composed of the loose sand prepared at the water content that was dry of optimum (i.e., Case C0L) which took only four hours in Phase 1 and Phase 3 (i.e., $t = 4$ h and i.e., $t = 28$ h) to fail—no failure occurred during Phase 2.

The bluff models C0L, C5L, C10L, WC0L, and WC5L which consisted of the looser material with a low fines content underwent two episodic failures. The number of failure reduced to only one failure—and even no failure for one case—as the strength of the beach and bluff forming material was enhanced through densification. For the looser material the strength enhancement was associated with the increase of the fines content beyond 10%, i.e., $\xi_f > 10\%$ when the initial water content was dry of optimum (i.e., Cases: C15L, C20L), and 5%, i.e., $\xi_f > 5\%$, when the soil was prepared at its optimum water content, i.e., Cases: WC10L, WC5L, WC20L. On the other hand, the bluff models constructed with the denser materials, irrespective of the fines content and moisture level, demonstrated a much higher erosion resistance and stability–no failure occurred for Case WC20D having all the ingredients for an enhanced soil strength. With the water content of $\omega = 7\%$ and $\omega = \omega_{opt}$ which are associated with an

unsaturated soil condition, the soil effective stress and, in turn, shear strength was boosted by to the matric suction (Holtz et al. 2003). This is believed to be the main stabilizing factor for the vertical-front buff of cohesionless constituent material (i.e., C0L, C0D, WC0L and WC0D). Nevertheless, the rise of the water level, in the following phase, which increased the soil moisture, weakened the surface tension-induced bonds among the soil particles and led to the reduction of the soil shear strength. Consequently, a rapid and extensive slope failure followed, particularly for the bluffs composed of the looser soils.

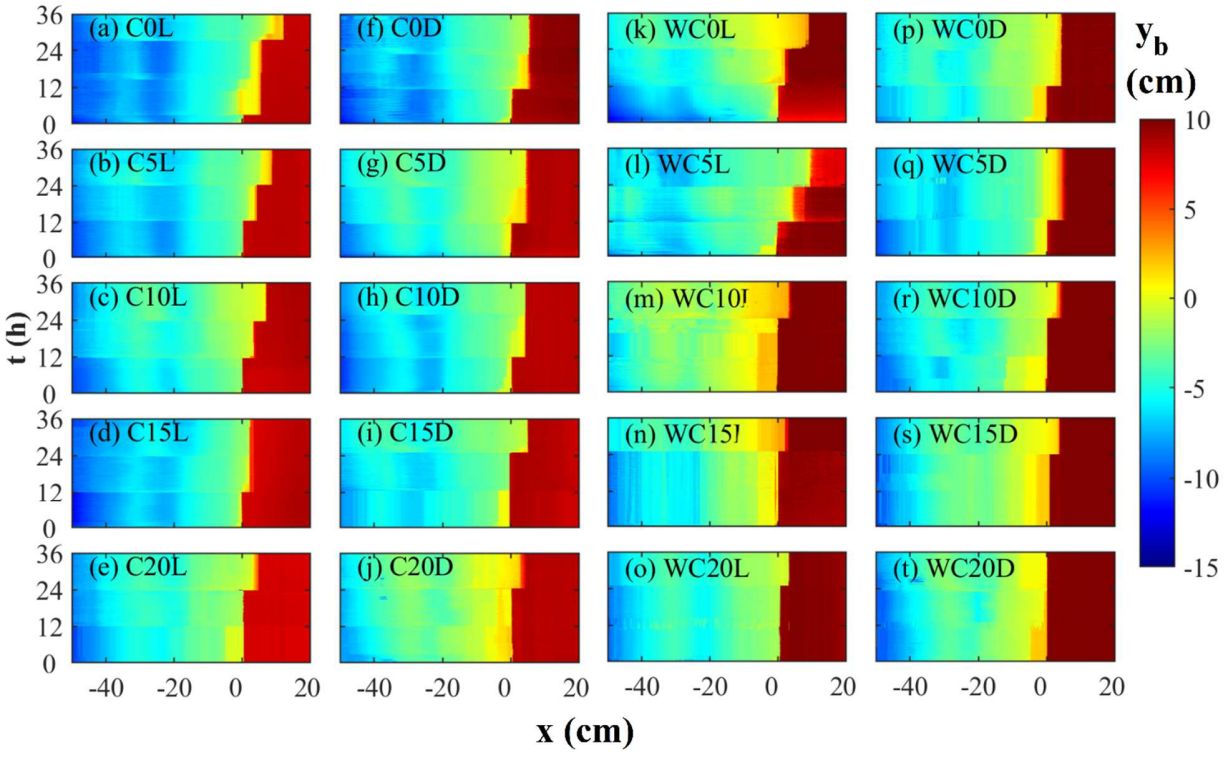

Figure 4. Spatial and temporal evolution of seabed and bluff morphology for twenty cases, color scale represents the bottom elevation (y_b)

The initial profile and final profiles for each phase, as well as the equilibrium beach profile, EBP (Bruun, 1954), associated with the mean water level are depicted in Figures 5 and 6. The figures show that, in general, the beach erosion rate was higher during Phase 1 compared to the following phases and that once the bluff failed, the wave energy was spent on transporting the resulting deposit offshore—a

temporary bluff erosion reduction mechanism. The offshore transport of the sediment deposit resulted in the rise of the bottom elevation at approximately x < -30. The volumes of the sediment deposited offshore and that supplied by the beach and bluff are different mainly because the deposited sediment is much looser than that of the original bed material. Further, the eroded fine-grained material remains in suspension.

The general beach profile varies for the different constituent materials. For the beach-bluff models of a larger fines content, the higher relative density and optimum water content, the nearshore beach profile appeared to follow a concave down curve while those with the looser or with a lower fines content materials, the profile curved concave up. As an example, Figure 7 highlights the evolution of the bottom profile for Cases C0L and C15D where the two distinct curvatures are marked using the dotted line. It is worth noting that the curves extend vertically from the bluff toe, Y= 0 m, down to the depth (r) which is on the order of the offshore incident wave height. Furthermore, it can be inferred from Figure 7 that the bluffs with the stronger constituent material underwent a sudden and major failure while the other one which has a weaker soil experienced multiple small episodic failures during the three phases.

The authors argued that the bluffs of looser and low fines content constituent material demonstrate little resistance against erosion owing to the reduced mechanical strength upon wetting (Ghazian Arabi et al., 2018 and 2020b). Here, the wave actions led to a rapid toe erosion and downcutting which undermine the slope stability of the bluff and cause shear failure when the soil was weak. On the other hand, the bluffs of a greater fines content, higher relative density, and optimum water content had a higher tensile strength. As a result, the bluff overhang induced by of the landward progression of the notch at the toe, resulted in a tensile failure. Table 4 summarizes the failure mode and the final length of recession for the 20 test cases. The results indicate that the failure mode dependents, among other factors, on the bluff material properties. This is consistent with the finding of Collins & Sitar (2008) and Arkin & Michaeli (1985).

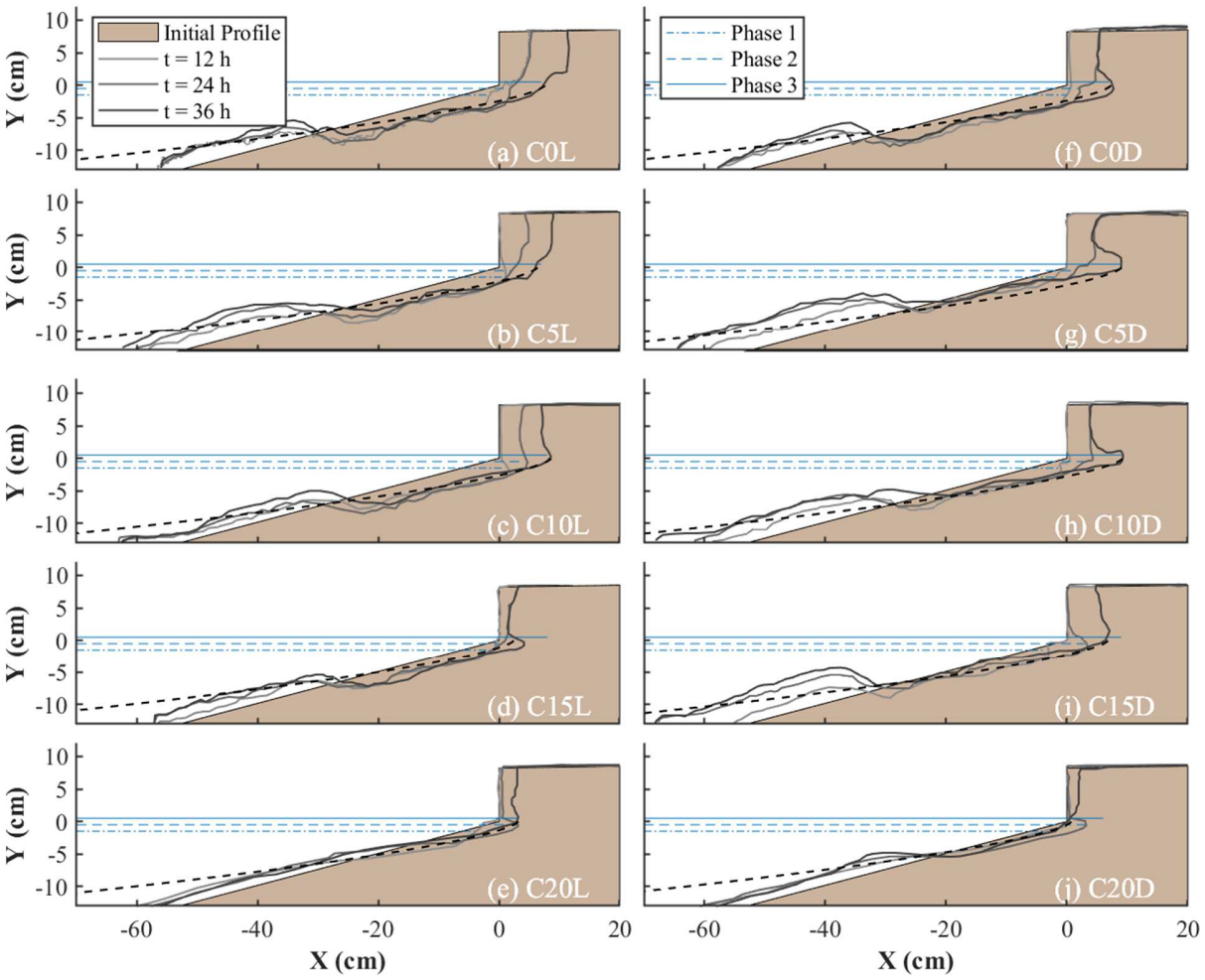

Figure 5. Cross-shore profiles for different time steps and for cases with dry water content (a) C0L, (b) C5L, (c) C10L, (d) C15L, (e) C20L, (f) C0D, (g) C5D, (h) C10D, (i) C15D, and (j) C20D. Water level (WL) is shown for Phases 1-3 using horizontal solid, dotted, and dashed lines. EBP is shown with the black dashed line.

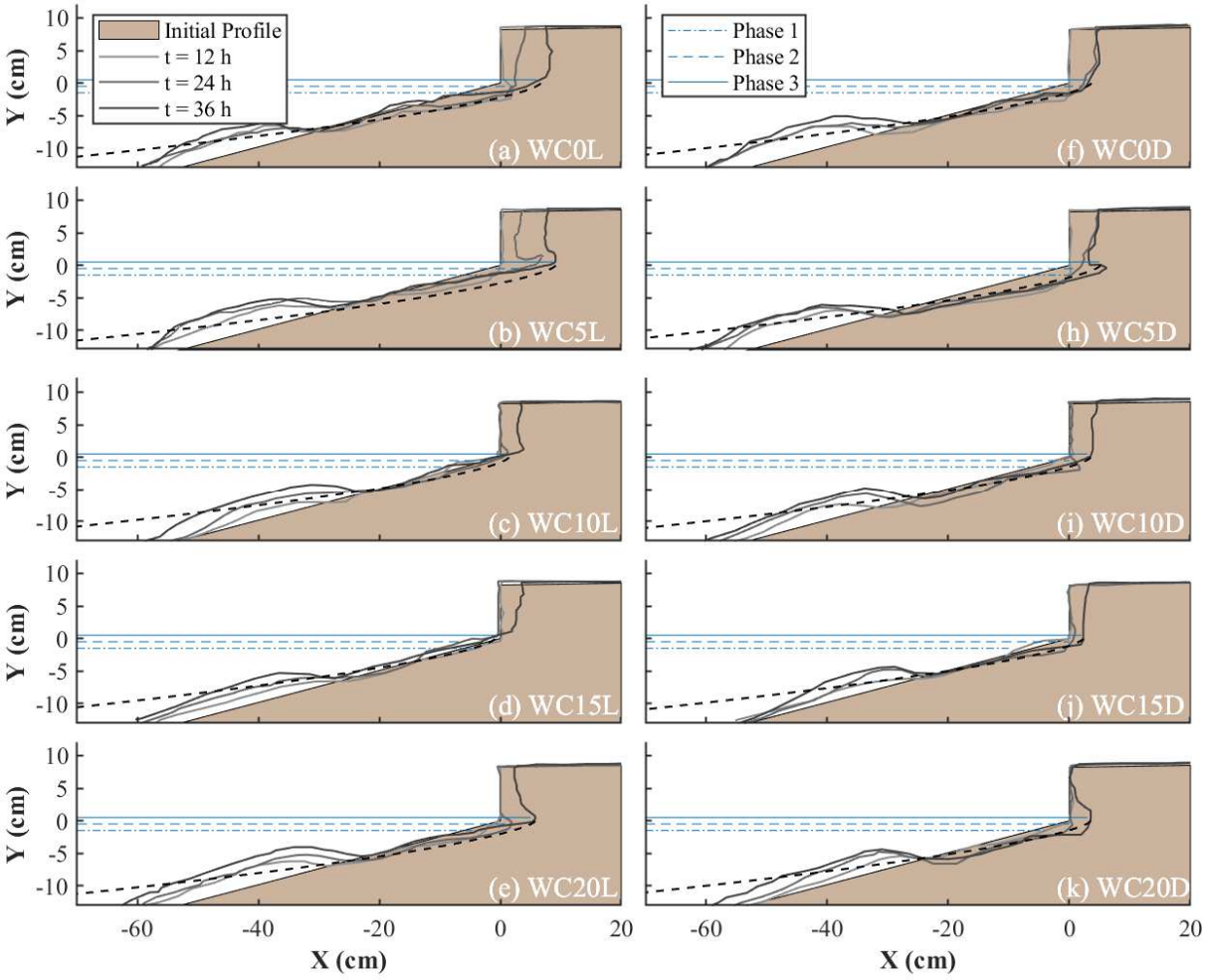

Figure 6. Cross-shore profiles for different time steps and for Cases with optimum water content (a) WC0L, (b) WC5L, (c) WC10L, (d) WC15L, (e) WC20L, (f) WC0D, (h) WC5D, (i) WC10D, (j) WC15D, and (k) WC20D. Water level (WL) is shown for Phases 1-3 using horizontal solid, dotted, and dashed lines. EBP is shown with the black dashed line.

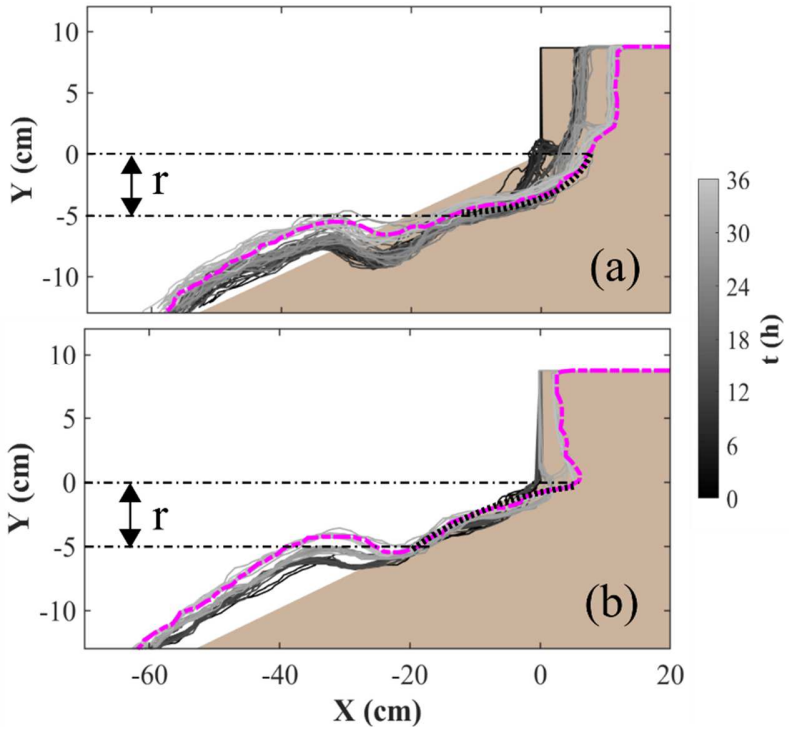

Figure 7. Evolution of beach-bluff profiles for (a) Case C0L, (b) Case C15D. Brown color shows initial bluff. Purple dashed line shows final profile. Thick black dotted curves show: (a) concave up, and (b) concave down. Dash-dotted lines indicate vertical range (r) of curves from bluff toe.

Table 4. Summary of failures characteristics

Case No.	Phase No.	Fines Content (%)	Packing	Moisture Condition	Failure Mode	Recession length (cm)
C0L	1	0	Loose	Dry	Shear	5.74
C0L	3	0	Loose	Dry	Shear	5.98
C5L	2	5	Loose	Dry	Shear	4.51
C5L	3	5	Loose	Dry	Shear	4.57
C10L	2	10	Loose	Dry	Tension	3.73
C10L	3	10	Loose	Dry	Tension	3.82
C15L	2	15	Loose	Dry	Tension	3.44
C20L	3	20	Loose	Dry	Tension	3.05
C0D	2	0	Dense	Dry	Tension	5.22
C5D	2	5	Dense	Dry	Tension	4.20
C10D	2	10	Dense	Dry	Tension	3.78
C15D	3	15	Dense	Dry	Tension	4.33
C20D	3	20	Dense	Dry	Tension	2.30
WC0L	2	0	Loose	Optimum	Tension	3.93
WC0L	3	0	Loose	Optimum	Tension	4.03
WC5L	2	5	Loose	Optimum	Tension	3.84
WC5L	3	5	Loose	Optimum	Tension	3.93
WC10L	3	10	Loose	Optimum	Tension	3.37
WC15L	3	15	Loose	Optimum	Tension	3.22
WC20L	3	20	Loose	Optimum	Tension	2.98
WC0D	2	0	Dense	Optimum	Tension	4.90
WC5D	2	5	Dense	Optimum	Tension	4.52
WC10D	3	10	Dense	Optimum	Tension	4.32
WC15D	3	15	Dense	Optimum	Tension	3.10
WC20D	-	20	Dense	Optimum	NA	0

3.3. *Bluff recession rate analysis*

Table 5 summarizes the breakdown of the measured bluff crest recession length for all the bluff models during each Phase. Also, the average recession rate, R_c, which is the ratio of the total recession length of the bluff crest to the test duration (i.e., 36 h) is presented. In general, the bluffs composed of the materials prepared at the optimum water content exhibited a reduced crest recession compared to those with the alternative water content. This reduction was more significant with the looser soil. For example, for the looser soil and 7% moisture ratio, adding only five percent fine-grained material to the cohesionless soil (i.e., from ξ_f = 0, C'=0 kPa to ξ_f = 5%, C'=1.01 kPa) resulted in more than 24% reduction in the recession rate. When the same soil was compacted at the optimum moisture, the bluff recession rate was less than that with the dryer soil (i.e., WC5L vs. C0L) but nearly the same as that of the cohesionless soil (i.e., WC5L vs. WC0L). The recession rate of the bluffs with the looser and dryer soil was reduced by about 70% from R_c= 0.33 cm/h to R_c= 0.1 cm/h when the fines content increased from ξ_f = 0 to ξ_f = 20% (and C' = 0 to C'= 5.12 kPa). Further, increasing the soil moisture of the looser soil with ξ_f = 20% to the optimum value (WC20L) resulted in a 63% recession rate reduction compared to the looser cohesionless soil with the optimum water content (WC0L).

The recession rate for the denser soils was different from the that of the looser soils. The increase of the fines content up to ξ_f = 20% did not make a noticeable difference in the recession rates of the bluffs composed of the dryer soil. However, when the water content increased to the optimum value, the recession rate was reduced rapidly with the increase of the fines content. In that case, a five percent fine-grained soil reduces the recession rate by about 8%. When the fines content was increased to 20%, the bluff did not fail, and thus no recession occurred.

The trend of the bluff recession, considering the soil's initial water content, relative density and fines content are visualized in Figure 8 where the recession rate (the vertical axes) is plotted as a function of the fines content (the bottom horizontal axis) and effective cohesion (the top horizontal axis). It can be clearly seen that the recession rate decreases with the increase of the effective cohesion. The data also

suggest that for a given fines content or alternatively an effective cohesion, the recession rate is significantly influenced by the relative density of the soil. The recession rate exhibits a trend with the effective cohesion like that with the fines content—a decreasing R_c with the increase of C'. The impact of the effective cohesion on the recession rate for the looser soil is significantly greater than that for the denser soil.

Table 5. Specification of bluff constituent material and corresponding recession

Case	Recession length (cm)				Recession Rate R_c (cm/h)
	Phase 1	Phase 2	Phase 3	Total	
C0L	5.74	0	5.98	11.72	0.33
C5L	0	4.51	4.57	9.08	0.25
C10L	0	3.53	3.82	7.35	0.20
C15L	0	3.44	0	3.44	0.10
C20L	0	0	3.05	3.44	0.10
C0D	0	5.22	0	5.22	0.15
C5D	0	4.20	0	4.20	0.12
C10D	0	3.78	0	3.78	0.11
C15D	0	0	4.33	4.33	0.12
C20D	0	0	2.3	4.33	0.12
WC0L	0	3.93	4.03	7.96	0.22
WC5L	0	3.84	3.93	7.77	0.22
WC10L	0	0	3.37	3.37	0.09
WC15L	0	0	3.22	3.22	0.09
WC20L	0	0	2.98	2.98	0.08
WC0D	0	4.90	0	4.90	0.13
WC5D	0	4.52	0	4.52	0.12
WC10D	0	0	4.32	4.32	0.09
WC15D	0	0	3.10	3.10	0.08
WC20D	0	0	0	0	0

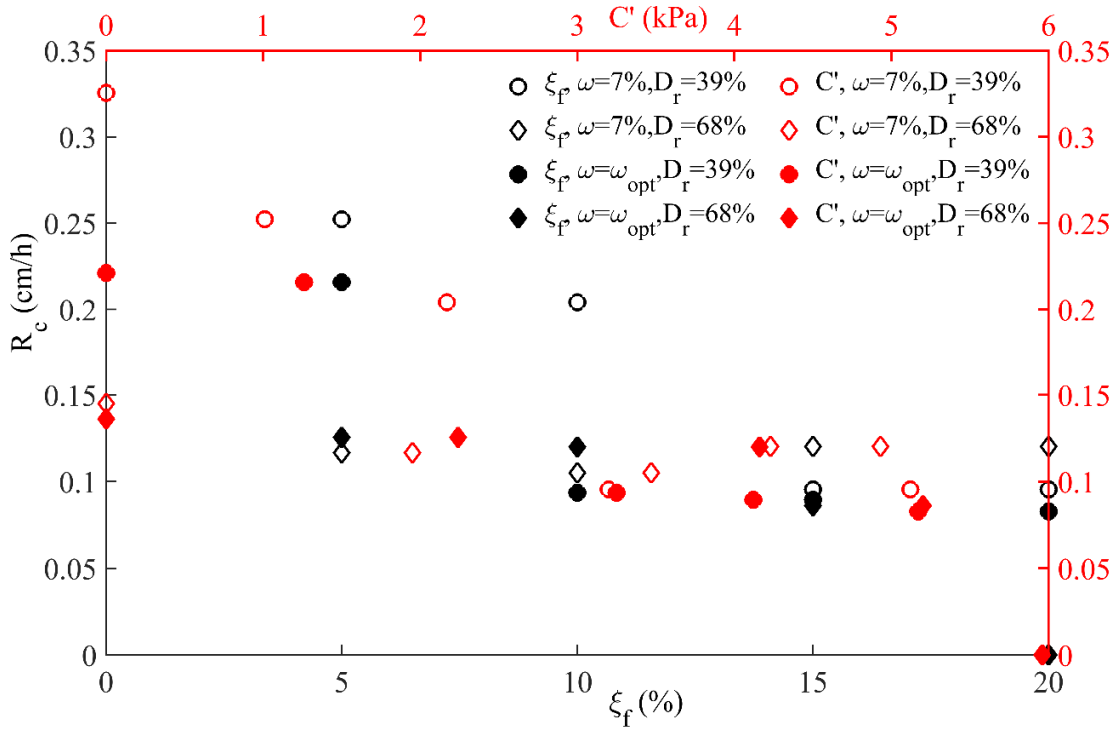

Figure 8. Bluff recession rate (R_c) versus fines content (ξ_f) and effective cohesion (C'). Black and red markers are associated with fines content (lower horizontal axis) and effective cohesion (upper horizontal axis), respectively.

By applying a multiple-regression analysis to the measured data, an empirical expression for recession rate was developed.

$$R_c = 0.51 + \xi_f\,(-0.0182 + 0.00023D_r) - 0.0044\,D_r - 0.0087\omega \quad (1)$$

The variables in Eq. (1) are in percentage, for example the fines content of 5, relative density of 39, and water content of 7 for C5L.

Figure 11 shows the agreement between the predicted and measured recession rates. The predicted values are shown to be strongly correlated with the measured recession rates with a coefficient of determination, R^2=0.83.

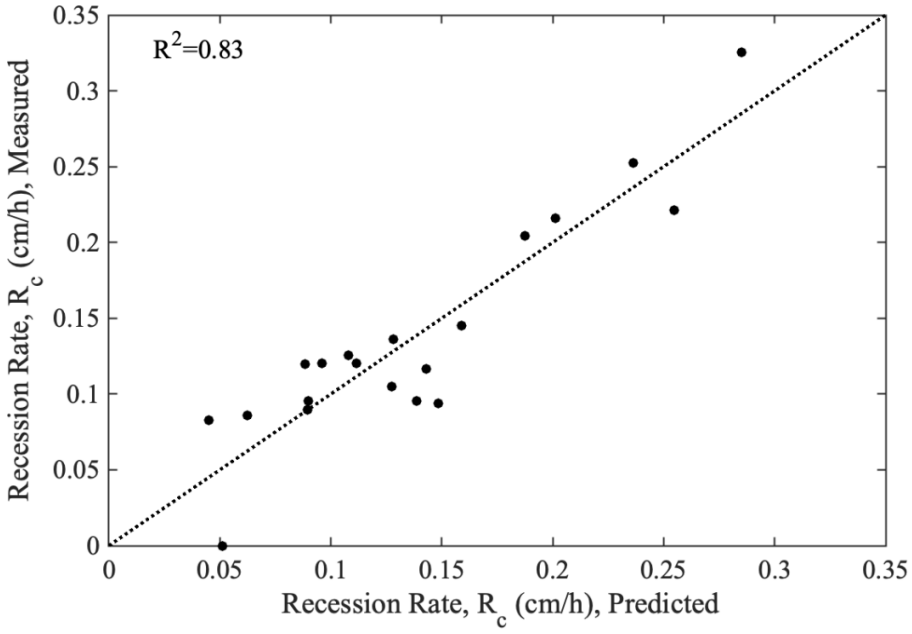

Figure 9. Comparison of measured and predicted recession rate as a function of fines content, relative density, and water content.

3.4. *Uncertainty quantification*

Natural beaches and bluffs' constituent materials often demonstrate heterogeneity in composition and mechanical properties. Further, human and instrument errors could lead to errors in soil sampling and testing outcomes. Thus, it is critical to assess the potential sensitivity of the empirical recession prediction formula to such uncertainties.

The general process of uncertainty quantification should contain the following steps (Joint Committee for Guides in Metrology, 2008): (1) identify the uncertainty parameters, x_i; (2) set up the model relationship, (3) identify the probability density function (PDF) for each parameter; (4) calculate

the uncertainty for each parameter; (5) combine the uncertainty of each parameter; (6) rank the factors that might have a significant effect on the results, and (6) determine the uncertainty. In the following, the Monte Carlo simulation is used for the uncertainty quantification.

3.4.1. Monte Carlo simulation

The fines content (ξ_f) and optimum water content (ω_{opt}) are correlated, for example, as increasing the fines content from 0 to 20% leads to an increase in the optimum water content from 9.5% to 13.2% (Table 2). Hence, a simple relationship using the linear regression, with strong correlation ($R^2 = 0.96$), is established between these two parameters.

$$\omega_{opt} = 0.2 * \xi_f + 9.34\% \quad (2)$$

where ω_{opt} and ξ_f are in percentage (%).

The Monte Carlo simulation requires running the model numerous times by substituting random input parameters based on their probability distributions. The three soil properties studied here are somehow interdependent as discussed earlier. To perform the Monte Carlo simulation two out of the three parameters are randomly generated in each run, based on a uniform distribution within the data range, while the third parameter is kept constant and set to its the median value (Table 6). The number of the iterations for each run is 10^5, following the recommendation by Garg (2019) and Joint Committee for Guides in Metrology (2008). The simulation results for the three runs are summarized in Table 6 and visualized in Figure 10. Run 1 shows the largest standard deviation (σ), and variance (Var), for the recession rate when the relative density is kept constant, but the fines content and initial water content are varying. The larger variance of Run 1 indicates that the changes in the initial moisture and fines content increase the recession rate's uncertainty range; while the variance becomes smaller when the relative density is varying (Runs 2 and 3).

Table 6. Summary of Monte Carlo simulation results

		Run 1	Run 2	Run 3
Input	D_r	54%	39% – 68%	39% – 68%
	ξ_f	0% – 20%	10%	3.8% – 20%
	ω_{opt}	7% – [0.2 F_c+9.34] %	7% – 11.34%	10.1%
Result	μ (R_c) (cm/h)	0.5050	0.5050	0.5046
	95% CI (R_c) (cm/h)	[0.5012, 0.5088]	[0.5037, 0.5064]	[0.5010, 0.5082]
	σ (R_c) (cm/h)	1.1×10^{-3}	3.825×10^{-4}	9.19×10^{-4}
	Var (R_c) $(cm/h)^2$	1.21×10^{-6}	1.46×10^{-7}	8.45×10^{-7}

μ, 95% CI, σ, and Var represent the mean; ninety percent of confident interval; and standard deviation of R_c.

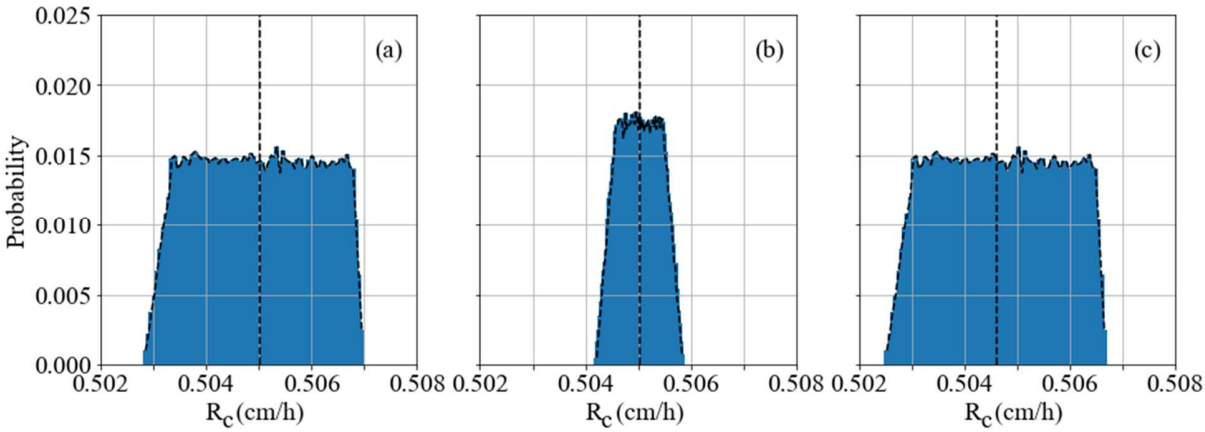

Figure 10. Probability distributions of R_c for: (a) Run 1, (b) Run 2 and (c) Run 3

3.4.2. Uncertainty propagation

Uncertainty propagation is defined as the effects on a function, Eq. (1), by the variable's uncertainty (water content, fine content and relative density) due to, for example, measurement limitation, instrumental precision and human errors. The uncertainty propagation is performed to quantify the potential influence of the input variables perturbation on the output parameters. Using the Monte Carlo simulation, the input parameters are selected randomly within an acceptable uncertainty range. The PDF of each input parameter is then identified empirically. Specifying the PDF for the Monte Carlo simulation

can be difficult when comprehensive data are lacking. Alternatively, decisions may be made based on expert opinions or reported values in the literature (Webster and Sokolov, 2000; Uzielli et al, 2008). Jones et al. (2002) and Uzielli et al. (2007) summarized the statistical ranges of the soil properties based on several previous studies which are partially listed in Table 7. The variability of each parameter is expressed as the coefficient of variation (COV) defined as the ratio of the standard deviation (σ) to the mean (μ), (i.e., $COV = \sigma/\mu \times 100\%$).

Table 7. Recommended soil parameters' statistical values

		Jones et al. (2002)		Uzielli et al. (2006)	
Soil Properties	Soil Type	NDG	COV (%)	NDG	COV (%)
ω	Fine-grained	40	18	NR	8~30
$D_{r\ a}$	Sand	5	19	NR	10~40
$D_{r\ b}$	Sand	5	61	NR	50~70

D_{r_a} represent the total variability for the direct method of determination; D_{r_b} represent the total variability for indirect determination; NDG: Number of data groups; and NR: Not reported.

Here the COV values of 20% and 19% are adopted for the water content and relative density, respectively. Due to the lack of recommendations in the literature for the fines content COV, a conservative value of $COV = 10\%$ is used. The COV of the input parameters and their corresponding means and standard deviations are listed in Table 8.

Table 8. Coefficient of variation for input parameters

Variable	Distribution	Mean	COV	σ
ξ_f	Gaussian	μ_{ξ_f}	10%	$\mu_{\xi_f} * 10\%$
D_r		μ_{Dr}	19%	$\mu_{Dr} * 19\%$
ω		μ_{ω}	20%	$\mu_{\omega} * 20\%$

The results of the uncertainty propagation are listed in Table 9 and visualized in Figures 11 and 12. The boxplots show that the confidence intervals for the 20 test cases are relatively similar. For the 20

bluff models, the averaged variance is found to be $2.88 \times 10^{-7}(cm/h)^2$ and the average 95% CI ranges between 0.5029 and 0.5072 (cm/h).

Table 9. Uncertainty propagation results

Case No.	$\mu(R_c)$ (cm/h)	$\sigma(R_c)$ $\times 10^{-4}\,(cm/h)$	$Var(R_c)$ $\times 10^{-7}(cm/h)^2$	95% CI(R_c) (cm/h)
1	0.5077	3.47	1.21	[0.5062, 0.5092]
2	0.5068	3.58	1.28	[0.5053, 0.5083]
3	0.5059	3.91	1.53	[0.5043, 0.5074]
4	0.5050	4.40	1.94	[0.5032, 0.5067]
5	0.5041	5.01	2.51	[0.5020, 0.5061]
6	0.5064	5.80	3.37	[0.5041, 0.5087]
7	0.5055	5.86	3.44	[0.5030, 0.5079]
8	0.5046	6.07	3.68	[0.5021, 0.5071]
9	0.5037	6.38	4.06	[0.5010, 0.5063]
10	0.5028	6.79	4.61	[0.5001, 0.5055]
11	0.5075	3.66	1.34	[0.5059, 0.5090]
12	0.5065	3.82	1.46	[0.5049, 0.5080]
13	0.5055	4.17	1.74	[0.5038, 0.5072]
14	0.5045	4.79	2.29	[0.5024, 0.5065]
15	0.5035	5.35	2.86	[0.5013, 0.5058]
16	0.5062	5.90	3.48	[0.5037, 0.5086]
17	0.5052	6.01	3.61	[0.5027, 0.5077]
18	0.5042	6.23	3.89	[0.5016, 0.5069]
19	0.5032	6.62	4.38	[0.5005, 0.5059]
20	0.5022	7.05	4.98	[0.4994, 0.5051]

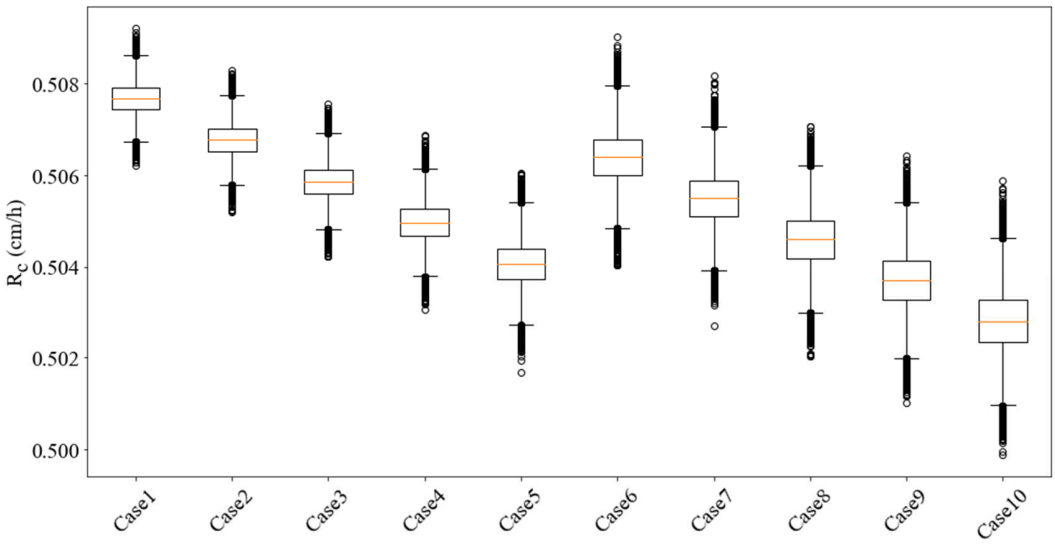

Figure 11. Boxplot of the uncertainty propagation for Cases 1~10.

142

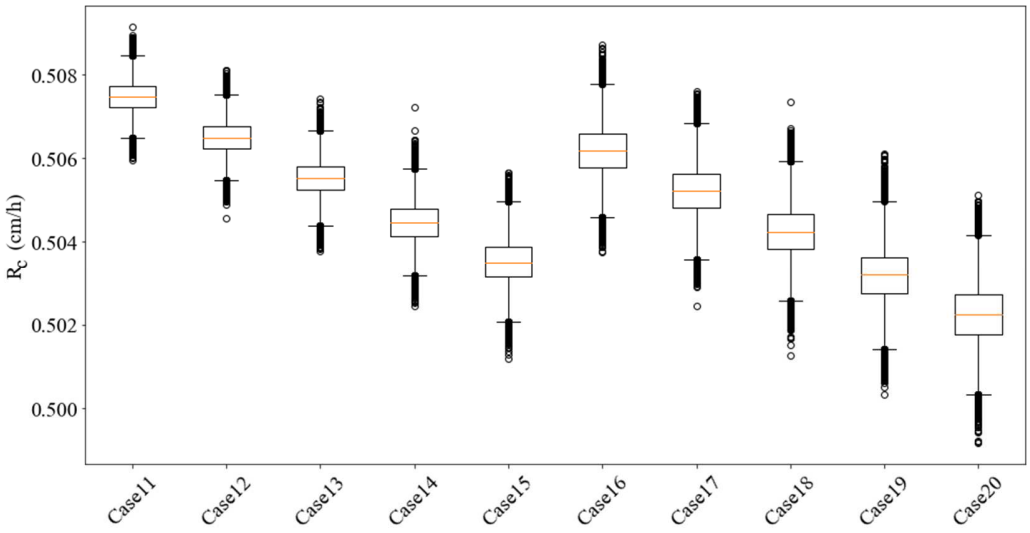

Figure 12. Boxplot of the uncertainty propagation for Cases 11~20.

143

144

145 Figure 13 shows, as an example, the simulation results for Case 13 (i.e., the bluff model WC10L
146 in Table 2) where the mean fines content, mean water content, and mean relative density are 10%, 11%,
147 and 39%, respectively. As shown in the figure, the recession rate follows a Gaussian distribution. To
148 quantify the correlation between the soil strength indices and recession rate, the correlation coefficients
149 are calculated based on the simulation results, and the distributions of the three input parameters are

plotted against that of the output—the recession rate—in Figures 14-16 using 2D a histogram heatmap. The correlation coefficients between the recession rates versus the fines content and the water content are calculated to be r = 0.43 and 0.46, respectively. However, a stronger correlation (r = 0.78) emerged between the recession rate and relative density. This is consistent with the earlier discussions highlighting a more prominent impact of the relative density on the recession rate compared to the other two variables.

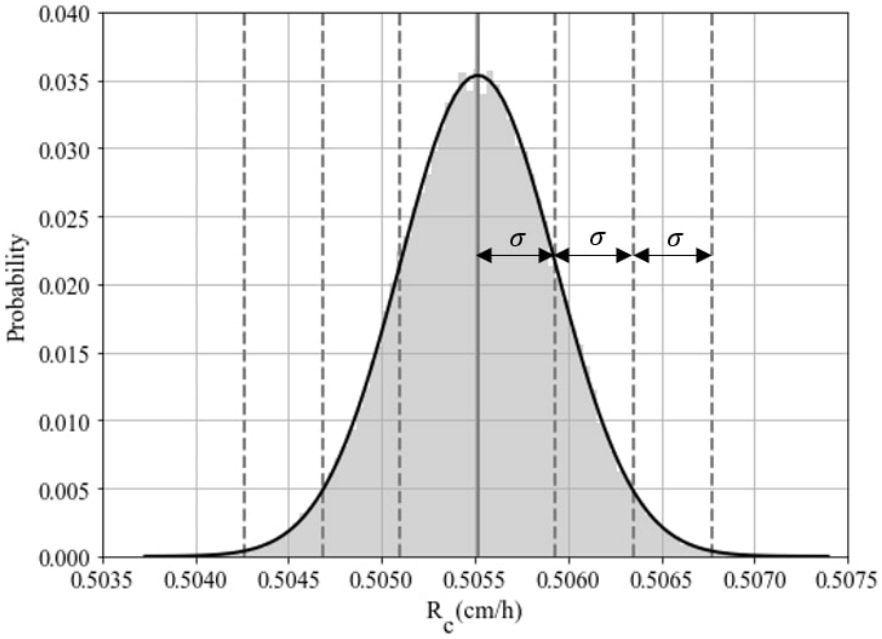

Figure 13. PDF of recession rate for Case 13 (WC10L)

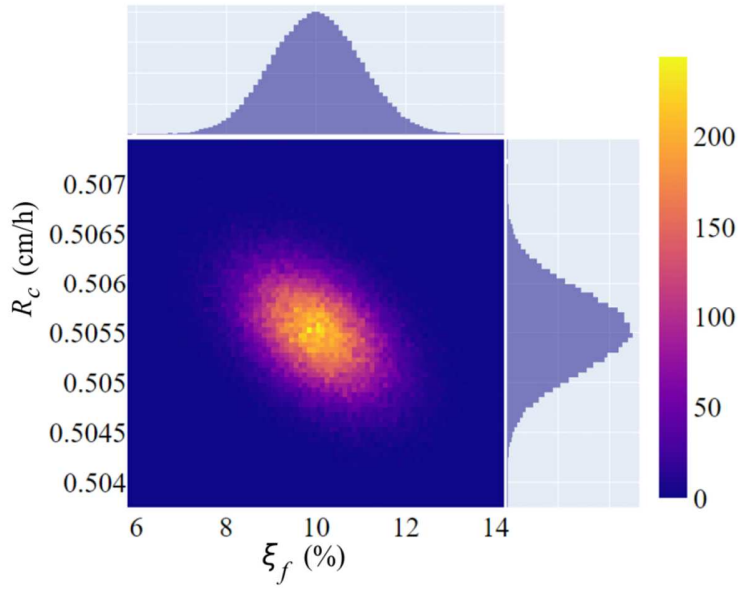

Figure 14. 2D-Histogram Heatmap between ξ_f and R_c for Case 13. The color bar represents the number of occurrences.

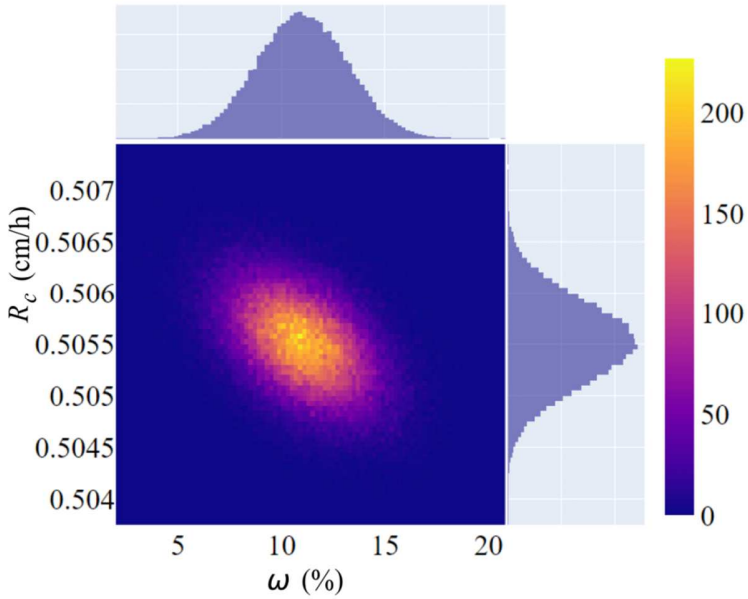

Figure 15. 2D-Histogram Heatmap between ω and R_c for Case 13. The color bar represents the number of occurrences.

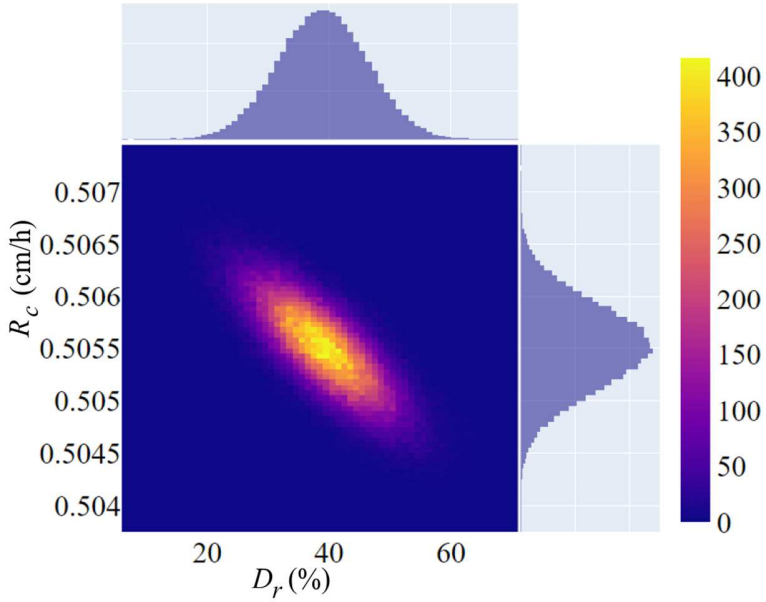

Figure 16. 2D-Histogram Heatmap between D_r and R_c for Case 13. The color bar represents the number of occurrences.

4. CONCLUSIONS

The beach and bluff models of varying constituent material composition and mechanical strength were subjected to incident waves and rising water levels for a total duration of 36 hours. The bluffs that consisted of the looser material of lower fines content, with the initial water content dry of optimum, underwent two episodic failures during the three phases of the test. The number of slope failures reduced as the mechanical strength of the beach and bluff forming material. On the other hand, the beach and bluff model constructed with the denser materials demonstrated a much greater erosion resistance and slope stability—irrespective of their fines content and moisture level. The slope failure of the bluffs composed of the denser material and/or a higher fines content, delayed until the water level was risen in the following phase. The matric suction contributed to an effective stress enhancement, increasing the shear strength of the material, and stabilizing the vertical-front bluffs of cohesionless constituent materials. The

rise of the water level, however, resulted in the soil moisture increase to a saturated or semi-saturated state, reducing the soil's shear strength and a rapid and extensive slope failure.

The foreshore beach profile for the models containing the materials of higher fines content, higher relative density, and those compacted at the optimum water content, followed a concave down foreshore profile while for the beach material of the lower density material or with a lower fines content, the beach profile was concave up. Both of those profiles extended vertically from the bluff toe, down to a depth that was on the order of the offshore incident wave height. The bluffs composed of the materials prepared at the optimum water content exhibited a reduced crest recession compared to those with the constituent materials dry of optimum. The recession rate of the bluff crest decreased with the increase of the effective cohesion—which increased with the fines content. For a given effective cohesion, the recession rate was significantly influenced by the relative density of the soil. The trends of the recession rate versus the effective cohesion were similar to that of the recession rate with the fines content. The impact of the effective cohesion on the recession rate for the bluff composed of the looser soil was significantly greater than that of the bluffs with the denser constituent material.

A predictive empirical relationship linking the recession rate to the fines content, relative density and water content has been proposed. Such relationship, when verified ad extended to include more soil properties, can quantify the influence of the soil composition on predicting the bluff recession for hazard mitigation or engineering design studies. The proposed relationship, however, is based on the limited number of experiments in this study and has its own limitations. These limitations are examined by an uncertainty quantification study.

Finally, employing the Monte Carlo simulations, the uncertainty quantification examining the effects of the variations in the fines content, relative density, and water content on the recession rate was carried out. The analysis confirms that the relative density is the most influential parameter for the recession rate. The quantified averaged variance was found to be ~$2.9 \times 10^{-7} (cm/h)^2$, with the average 90% confidence interval ranging between 0.504 and 0.506 (cm/h). This uncertainty was determined based on the variability of the input parameters recommended by the previous literatures.

Several aspects of bluff erosion and recession have not been addressed within this limited scope study which could be subjects of future studies. For instance, a broader range of soil properties and flow conditions needs to be considered. Further, processes such as intermittent wetting and drying and their effects on the strength of bluff forming materials and in turn on the slope stability require a special attention. Heterogeneity in bluff constituent materials and its impact on the bluff recession is another important topic to be studied. It is also critical to study bluff erosion and recession process through field investigations in order to quantify the scale effects.

Acknowledgement

This study was funded by National Oceanic and Atmospheric Administration, New York Sea Grant, Award No. 80794.

REFERENCES

Arkin, Y. and Michaeli, L. (1985). Short- and long-term erosional processes affecting the stability of the Mediterranean coastal cliffs of Israel," *Eng. Geol.*, vol. 21, no. 1–2, pp. 153–174, May, doi: 10.1016/0013-7952(85)90003-1.

ASTM D4767-11. (2011). ASTM D4767 – 11. Standard Test Method for Consolidated Undrained Triaxial Compression Test for Cohesive Soils. American Society for Testing and Materials, 1–11. https://doi.org/10.1520/D4767-11.2.

ASTM D698-12e2, A. (2012). ASTM D698-12e2, Standard Test Methods for Laboratory Compaction Characteristics of Soil Using Standard Effort (12 400 ft-lbf/ft3 (600 kN-m/m3)). American Society for Testing and Materials.

Battjes, J.A. (1974). Surf similarity. Proceedings 14th International Conference on Coastal Engineering, pp. 466–480, doi:10.9753/icce.v14.

245 Bruun, P., (1954), Coast erosion and the development of beach profiles, Beach erosion board technical
246 memorandum. No. 44. U.S. Army Engineer Waterways Experiment Station. Vicksburg, MS.
247 Buckler, W., and Winters, H. (1983). Lake-Michigan bluff recession. Ann. of the Assoc. of Amer. Geog.,
248 73, 89–110.
249 Carter, R. W. G., Johnston, T. W., McKenna, J., and Orford, J. D. (1987). Sea-level, sediment supply and
250 coastal changes: Examples from the coast of Ireland. Progress in Oceanography, 18(1–4), 79–101.
251 https://doi.org/10.1016/0079-6611(87)90027-9.
252 Castedo, R., Fernández, M., Trenhaile, A., and Paredes, C. (2013). Modeling cyclic recession of cohesive
253 clay coasts: Effects of wave erosion and bluff stability. Marine Geology, 335, 162–176.
254 https://doi.org/10.1016/j.margeo.2012.11.001.
255 Chen, Z., Zhou, J., and Wang, H. (1994). Soil Mechanics. Tsinghua University Press.
256 Collins, B., and Sitar, N. (2008). Processes of coastal bluff erosion in weakly lithified sands.
257 Geomorphology, 97, 483–501. https://doi.org/10.1016/j.geomorph.2007.09.004.
258 Collins, B., and Sitar, N. (2009). Geotechnical properties of cemented sands in steep slopes. Journal of
259 Geotechnical and Geoenvironmental Engineering, 135(October), 1359–1366.
260 https://doi.org/10.1061/(ASCE)GT.1943-5606.0000094.
261 Damgaard, J., and Dong, P. (2004). Soft cliff recession under Oblique Waves: Physical Model Tests. J.
262 Waterway, Port, Coastal, Ocean Eng., 2004, 130(5), 234–242.
263 Duijsings, J. J. H. M. (1987). A sediment budget for a forested catchment in Luxembourg and its
264 implications for channel development. Earth Surface Processes and Landforms, 12(2), 173–184.
265 https://doi.org/10.1002/esp.3290120207.
266 Farhadzadeh, A. and Ghazian Arabi, M. (2020). Linking geomechanical characteristics of soil with
267 erosion of steep shore and recession of bluff, AGU Fall Meeting 2020.
268 Garg, N., Yadav, S., and Aswal, D.K. (2019). Monte Carlo simulation in uncertainty evaluation: Strategy,
269 implications, and future prospects. MAPAN 34, 299–304. https://doi.org/10.1007/s12647-019-
270 00345-5.

271 Ghazian Arabi, M., and Farhadzadeh, A. (2022). "Characterizing incipient motion of low fines content
272 soils with varying compositions, water contents, and relative densities, International Journal of
273 Sediment Research, March 2022, https://doi.org/10.1016/j.ijsrc.2022.03.002.
274 Ghazian Arabi, M., Farhadzadeh, A., and Khosravi, M. (2020a). Erosion and recession of beach-bluff
275 system of low fine content due to wave and surge actions. In Geo-Congress 2020 (pp. 779–787).
276 https://doi.org/10.1061/9780784482810.081.
277 Ghazian Arabi, M., Farhadzadeh, A., and Khosravi, A. (2018). Recession of predominantly sandy bluffs.
278 36th International Conference on Coastal Engineering (ICCE2018), Baltimore, MD.
279 Ghazian Arabi, M., Khosravi, M., and Farhadzadeh, A. (2020b). Effects of fines content and relative
280 density on erosion and recession of predominantly sandy beach-bluff system. Journal of Waterway,
281 Port, Coastal, and Ocean Engineering. https://doi.org/10.1061/(ASCE)WW.1943-5460.0000625.
282 Hanson G. (1990) Surface Erodibility of Earthen Channels at High Stresses part I - Open Channel
283 Testing. Transactions of the ASAE. 33 (1): 0127-0131. http://doi/10.13031/2013.31305.
284 Hapke, C., Reid, D., and Richmond, B. (2009). Rates and trends of coastal change in California and the
285 regional behavior of the beach and cliff system. Journal of Coastal Research, 253, 603–615.
286 https://doi.org/10.2112/08-1006.1.
287 Jones, Allen L., Steven L. Kramer, and Pedro Arduino (2002). Estimation of uncertainty in geotechnical
288 properties for performance-based earthquake engineering, Pacific Earthquake Engineering Research
289 Center, College of Engineering, University of California.
290 Kamphuis, W. (1990). Influence of sand or gravel on the erosion of cohesive sediment. Journal of
291 Hydraulic Research., 28(1), 37–41.
292 Ladd, R.S. (1978). Preparing test specimens using undercompaction. Geotech. Testing J., 1(1), 16-23.
293 Lonnie, T. (1977). A Mineralogical Study of Long Island Clays. Thesis, Adelphi University.
294 Mitchener H. and Torfs H. (1996). Erosion of mud / sand mixtures, Coastal Engineering, 29, 96, 1–25.
295 Newson, T., Sentenac, P., Dong, P., Wu, X., and Davies, M. (2006). Modelling failure mechanisms of
296 soft cliff profiles. International Conference on Protection and Restoration of the Environment VIII.

297 Rinaldi, M., and Casagli, N. (1999). Stability of streambanks formed in partially saturated soils and
298 effects of negative pore water pressures: The Sieve River (Italy). Geomorphology, 26(4), 253–277.
299 https://doi.org/10.1016/S0169-555X(98)00069-5.
300 Rohan, K., Lefebvre, G., and Douville, S. (1980). Erosion mechanisms of intact clay (in French).
301 Proceedings of the Candian Coastal Conference, 200-219.
302 Skafel, M., and Bishop, C. (1994). Flume experiments on the erosion of till shores by waves. Coastal
303 Engineering, 23, 329–348.
304 Sunamura, T. (1976). Feedback relationship in wave erosion of laboratory rocky coast. J. Geol., 84, 427–
305 437.
306 Swenson, M., Wu, C., Edil, T., Mickelson, D., Swenson, M., Wu, C., Edil, T., and Mickelson, D. (2006).
307 Bluff recession rates and wave impact along the Wisconsin coast of Lake Superior. International
308 Association for Great Lakes Research, 32(3), 512–530.
309 Trenhaile, A. (2009). Modeling the erosion of cohesive clay coasts. Coastal Engineering, 56(1), 59–72.
310 https://doi.org/10.1016/j.coastaleng.2008.07.001.
311 Uzielli, M.,Lacasse, S., Nadim, F., and Phoon, K.K. (2007). Soil variability analysis for geotechnical
312 practice. Characterisation and Engineering Properties of Natural Soils, 3-4: 1653-1752.
313 ScholarBank@NUS Repository.
314 Uzielli M, Nadim F, Lacasse S, and Kaynia A.M. (2008). A conceptual framework for quantitative
315 estimation of physical vulnerability to landslides. Eng Geol 102:251–256.
316 Vallejo, L., and Degroot, R. (1988). Bluff response to wave action. Engineering Geology, 1(16), 1–16.
317 https://doi.org/10.1590/S1516-18462008000300012.
318 van Ledden, M., Van Kesteren, W. G., & Winterwerp, J. C. (2004). A conceptual framework for the
319 erosion behaviour of sand-mud mixtures. Continental Shelf Research, 1–11.
320 Wan, C. F., and Fell, R. (2004). Investigation of rate of erosion of soils in embankment dams. Journal of
321 Geotechnical and Geoenvironmental Engineering, 23(40), 1390–1392.
322 https://doi.org/10.1061/(ASCE)1090-0241(2004)130.

Webster, M.D., and A.P. Sokolov (2000). A methodology for quantifying uncertainty in climate projections. Climatic Change, 46(4):417-446 http://dx.doi.org/10.1023/A:1005685317358.

Yao P., Hu Z., Su M., Chen Y., and Ou S. (2018), Erosion Behavior of Sand-silt Mixtures: The Role of Silt Content. Journal of Coastal Research, 85, 1171–1175, https://doi.org/10.2112/SI85-235.